Heritage Science

RESEARCH

Open Access

Analysis of the seismic isolation characteristics of the overall friction pendulum bearing (OFPB) of a pagoda under three types of seismic actions

Qing He[1], Dewen Liu[1,2*], Min Lei[3*], Xiaopeng Li[1] and Haoxuan Wu[1]

Abstract

In this study, the seismic performance of an ancient pagoda with significant historical and cultural values in China is upgraded by using overall friction pendulum bearing (OFPB) seismic isolation technology, This technique can be used to isolate the pagoda without damaging it. By implementing the OFPB seismic isolation retrofit on the pagoda and comparing and analyzing it with the unretrofitted seismic model, the response of the pagoda under the action of nine seismic waves of three types, namely, near-field earthquakes, far-field earthquakes, and common earthquakes, is investigated. The results show that the OFPB seismic isolation technique significantly reduces the seismic response of the ghats, in which the acceleration amplification factor is reduced by a maximum of 82.46%, the inter-story displacement is reduced by a maximum of 85.15%, and the base shear force is reduced by a maximum of 96.76%. In addition, the tensile damage of the ghats with OFPB seismic isolation was significantly controlled. While the model without seismic isolation has serious damage under the same seismic action and even faces the risk of collapse. The results of the study confirm that the OFPB seismic isolation technology plays a key role in improving the seismic performance of the tower, which is of great theoretical and practical significance to the protection of the tower, and provides an effective technical way for the protection of the tower in the seismic-prone areas.

Keywords Ancient masonry towers, Dynamic characteristics, Earthquake response, Damage analysis, ABAQUS

Introduction

As an important part of the world's cultural heritage, ancient pagodas not only carry rich historical and cultural values but also are the crystallization of architectural art and engineering technology [1]. However, most of the ancient pagodas are located in earthquake-prone areas, and frequent seismic activities pose a serious threat to their structural safety [2, 3]. Historically, many ancient pagodas suffered different degrees of damage or even collapsed completely during earthquakes, resulting in irreversible loss of cultural heritage [4]. Therefore, it is of great practical significance and far-reaching historical value to study the seismic performance of ancient pagodas, especially the seismic isolation and reinforcement technology. Chavez et al. [5] conducted shaking table experiments to provide basic information for calibration and analysis of the model. Anzani et al. [6] studied damaged towers in Italy and proposed methods to evaluate the protection status and time evolution of ancient buildings. Lee et al. [7] compared the measured intrinsic

*Correspondence:
Dewen Liu
civil_liudewen@sina.com
Min Lei
xnjdleimin@163.com
[1] College of Civil Engineering, Southwest Forestry University, Kunming 650000, Yunnan, China
[2] Kirik University, Bangkok, Thailand
[3] College of Civil Engineering, Southwest Jiaotong University, Chengdu 610000, Sichuan, China

frequencies of the stone tower with the finite element model, and subsequently, the experimental data were compared with the PGA from the FEM analysis, and an average difference of 13% was found, and the structure demonstrated that it is possible to predict the dynamic characteristics of this type of structure by the finite element method. De Iasio [8] et al. developed a complete model of the Longhu Pagoda in China using ABAQUS and proved the accuracy of the results obtained from the pushover by nonlinear dynamic analysis. The accuracy of the results obtained from the analysis provides useful information about crack extension that confirms the post-earthquake damage of the tower, finally, using the dynamics theorem of the limit analysis, the collapse mechanism and the rate of collapse of the tower are investigated, and the ability to predict earthquake damage is discussed. Shakya et al. [9] conducted an earthquake vulnerability assessment for pagoda temples with important historical and heritage values in Nepal, and used a simplified method and vulnerability index to assess more than 78 temples in Kathmandu Valley. Assessment results, databases, and damage classifications are integrated into GIS tools, enabling spatial visualization of damage scenarios to help plan retrofits to mitigate earthquake risks. Lu J et al. [10] took Xuanzang Tower as an example, tested the 1/8 scale model with a shaking table, and compared it with the finite element simulation results. The results showed that the acceleration amplification coefficient and the displacement results were slightly different but basically consistent, and explained that this phenomenon was due to the crack of the masonry itself having a certain influence on the dynamic response of the structure. Wang P et al. [11] took Chinese masonry towers as an example to study the rapid assessment of the seismic resistance of existing masonry towers, which is of great significance for the detailed assessment of the safety of pagodas. Ponsi et al. [12] evaluated the computational efficiency and accuracy of the two methods by comparing the models of two brick towers with the deterministic and Bayesian methods. By updating the deterministic model with the algorithm assisted by the agent model for multi-objective optimization, the calculation cost and result quality were compared. A reliable Bayesian model can be obtained by proper selection and calibration of proxy model. Lu J et al. [13, 14] used the flexural curvature method to identify and analyse the seismic damage of Baiyun Tower, and the dynamic characteristics of the tower were obtained by means of field testing and compared with the results of numerical simulation. The results show that the first-order intrinsic frequencies of the simulation results are close to each other, and the main tensile stress distributions under different earthquakes are similar, while the seismic damage distributions are slightly different. The seismic damage is more serious in the middle and lower two layers, and the accumulation of seismic damage in the first layer is more obvious. Wu X et al. [15] established the overall model and layered model of the bottle-shaped pagoda of Mafosi Temple through ABAQUS software for analysis, and found that the tensile damage factor and the main tensile stress at the bottom of the tower exceeded the limiting value, and the top of the pagoda had serious stiffness degradation under the action of the large earthquake, and the conclusion revealed the seismic weak parts of the pagoda. Wang P et al. [16] proposed a three-dimensional limit analysis model to analyze the collapse and failure of giant masonry structures under earthquake action. Based on structural discretization, the model estimates collapse loads through linear programming, and takes three ancient pagoas in China as examples to verify the model, which quickly and accurately estimates the bearing capacity and complex failure mechanism. Xu D et al. [17] studied the influence of inclination Angle on seismic performance of historical masonry towers through 1/8 scale model shaking table test. It is found that the tilt significantly reduces the resonance frequency, increases the equivalent damping ratio, and increases the acceleration and displacement response, indicating that the tilt has a significant effect on seismic performance. Li M et al. [18] used 3DEC software to simulate the response of ancient masonry pagodas in the Tang Dynasty under earthquake action, and found that the middle floors of ancient pagodas were vulnerable under a 7-degree earthquake, the top floors collapsed first, and then the floors began to collapse from the bottom up. The study provided insights for predicting their seismic performance and collapse risk. Tian P et al. [19] studied the improvement of the shear strength of glutinous rice lime mortar. Through shear test and scanning electron microscope analysis, they found that 2 wt % Na-SiO2 and 0.5% fiber additives significantly enhanced the shear strength and toughness of mortar, while the mixture of sand and clay aggregate improved the capacity and ductility of mortar. Providing insights into the restoration of historic buildings. Hu J et al. [20] explored the dynamic characteristics of an ancient masonry tower by in-situ tests and finite element simulations, taking Huilong Pagoda in Yongzhou, Hunan Province as an example. The analysis results show that the numerical model analysis results of ANSYS software are in good agreement with the measured values, which confirms the validity of the developed numerical simulation method. Xie Q et al. [21] analyzed the dynamic characteristics and seismic performance of representative towers in ancient China by means of the shaking table tests on a 1/8 scale masonry model. The experiments involved four different

scale earthquake simulations in two directions, revealing the dynamic characteristics and damage mechanisms of the towers. Further macroscopic simulations using a nonlinear finite element model show good agreement with the experimental results. The findings provide important insights into understanding the seismic behaviour of historic masonry structures. Pham et al. [22] used ANSYS software for 3D finite element modelling and combined it with dynamic centrifuge testing to evaluate the seismic performance of the Seokga Pagoda of the Silla Dynasty period in Korea.Seismic behaviour assessments such as vibration patterns and time domain signals were carried out, and finally verified by the results of centrifuge testing. Tang Y et al. [23] investigated the effect of the tilting of an ancient pagoda in China on the distribution of the soil stresses underneath it by studying the properties of two soils (muddy clay Q4 and ancient clay), and established a mathematical model to estimate the residual strain of the soil by measuring the deformation.

For the research on seismic damping and strengthening of pagodas, Li S et al. [24] repaired and refurbished the East Pagoda of Yongzuo Temple and tested its dynamic characteristics, providing a method for identifying structural weaknesses. Mason et al. [25] strengthened a tower around 1860 in the U.S.A. Li T et al. [26], using the Xiaoyan Pagoda as an example, developed twelve types of Shape Memory Alloy (SMA)-based suspension pendulum damping systems (SMA-SPDS). Hao W et al. [27] evaluated the effectiveness of different vibration-damping schemes through shaker tests and numerical analysis. The results showed that GFRP reinforcement can effectively improve seismic performance, inhibit step cracking, and change the damage mode from brittle to ductile. Pan Y et al. [28] studied the effects of different seismic isolation schemes on the seismic performance of brick towers using the Zhenguo White Tower in Pengzhou as an example. It was found that the use of larger seismic isolation bearings and optimal arrangement can significantly reduce the seismic response, the maximum acceleration at the top is reduced by about 80%, and the horizontal shear force is reduced by about 70%, which effectively improves the seismic safety of the tower. Based on the above research literature, in order not to damage the pagoda itself and better ensure the integrity of the protected building, this study proposed the integral friction pendulum support (OFPB) to study the pagoda isolation and discussed the isolation performance of OFPB to the pagoda. To ensure the accuracy of the research content, three types of earthquakes, namely near-field earthquakes, far-field earthquakes, and ordinary earthquakes, are chosen to analyze the seismic resistance and isolation model of the pagoda, and the dynamic response mechanism of the pagoda using OFPB seismic isolation is investigated.

Materials and methods

Bai Lang Feng Shui tower overview

Bai Lang Feng Shui Tower is located in Nanming District, Guiyang City, Guizhou Province, is an ancient building with important historical and cultural value, the tower is made of brick, as shown in Fig. 1. The total number of layers of the structure is nine, the height of the structure is 22.5 m, hexagonal, the height of each layer decreases with the rise of the floor, in addition to the ground floor of the south face of a door, the rest of the face is open with a coupon hole, the whole tower a total of fifty-three coupon holes. Detailed dimensions as shown in Table 1,

(a) Pagoda full view (b) Pagoda Coupon Cave (c) Pagoda Doorway

Fig. 1 Bai Lang Feng Shui Pagoda Real Picture

Table 1 Detailed dimensions of Bai Lang Feng Shui Tower/m

Floor	Floor height	Floor elevation	Pagoda length	Stacked edge length	Wall thicknesses	Hole width	Hole height
0	2.40	2.40	2.80	/	/	/	/
1	4.20	6.60	2.18	3.22	1.26	0.60	1.60
2	3.10	9.70	1.90	2.09	0.95	0.55	1.45
3	2.50	12.20	1.68	1.86	0.82	0.55	1.15
4	2.20	14.40	1.48	1.67	0.70	0.50	1.00
5	1.90	16.30	1.31	1.50	0.59	0.45	0.95
6	1.60	17.90	1.16	1.35	0.50	0.40	0.85
7	1.40	19.30	1.02	1.21	0.42	0.35	0.75
8	1.30	20.60	0.90	1.09	0.35	0.30	0.65
9	1.90	22.50	0.80	/	0.28	0.25	0.55

of which layer number 0 is the tower foundation, a doorway.

The model established and selection of earthquakes

Model established

In this study, a 1:1 3D solid model was built using Solid Works software based on the measured data of the Pendulum wind and water tower in meters as shown in Fig. 2a. The model was imported into the finite element analysis software ABAQUS for numerical analysis, and the Newton–Raphson method in the ABAQUS/Standard module was used to solve the system of nonlinear equations. The pagoda cell meshing type is a C3D4 cell, the mesh size is 0.35, and the curvature control sets the maximum deviation factor to 0.1. The total number of delineated nodes is 9357 and the total number of units is 39,269. Considering that the pagoda is made of brick, which is consistent with most ancient buildings, reference [15] defines the method of material parameters, conducts experiments based on bricks of the same material as the pagoda picked up near the pagoda, and calculates the detailed parameters of the brick through clustering analysis of the damage forms of the bricks. The density ρ of the brick is 1900 kg/m3, the elastic modulus E is 1800 MPa, and the Poisson ratio υ is 0.15. Considering that the damage characteristic of bricks is brittle damage, the Concrete Damage Plasticity (CDP) intrinsic model is used to simulate this damage characteristic [8, 21], and the principle of energy equivalence is used to approximate the damage parameters, so as to simulate the damage characteristics of the material, Fig. 3 shows the tensile compression and the stiffness recovery of the concrete in this process. The plastic damage parameter expansion angle is taken as 30°, eccentricity is taken as 0.1, the ratio of biaxial to uniaxial compressive strength is taken as 1.16, the ratio of the second stress invariant on the tensile and compressive meridians is taken as 0.6667, and the viscosity parameter is 0.0005.

Overall friction pendulum bearing modeling

Overall Friction Pendulum Bearing (OFPB) seismic isolation is a system in which the entire structure is placed on top of the slider, similar to a large 'tumbler'. Specifically, the system dissipates the energy of an earthquake through friction between the slider and the slipway, thus ensuring the safety and stability of the structure. The radius of curvature and depth of the slider and the chute are calculated based on the dimensions of the base of the pagoda to ensure that the slider can completely take up the pagoda. In this paper, the curvature radius of the slide block and slide is 22 m, the thickness of the slide block is 0.2 m, the maximum thickness of the slide is 0.4 m, and the minimum thickness of the slide is 0.2 m. The 3D solid model of the support is established by ABAQUS software, as shown in Fig. 2b. The meshing type is C3D8R cell, the mesh size is 0.21, and the curvature control sets the maximum deviation factor to 0.1. The total number of nodes divided by the slider is 2292 and the total number of units is 1628, and the total number of nodes divided by the slide is 2379 and the total number of units is 1496. The support is manufactured using steel, in practice, due to the large size of the support and slider, can be obtained by designing and manufacturing a number of small pieces of splicing, which is conducive to the manufacture and transport of the support. In this paper, the elastic modulus E of steel is taken as 2.0×105Mpa, the density ρ is taken as 7.8×103 kg/m3, the Poisson ratio is taken as υ 0.3, the yield strength is taken as 3.35×102 MPa, and the ultimate strength is taken as 4.00×102 MPa. According to previous experience, the friction coefficient between the slider and the slide can be controlled by the use of lubricants. In this study, the friction between the slider and the slide is simulated by Coulomb friction, regardless of the change between the speed and the friction coefficient. The normal

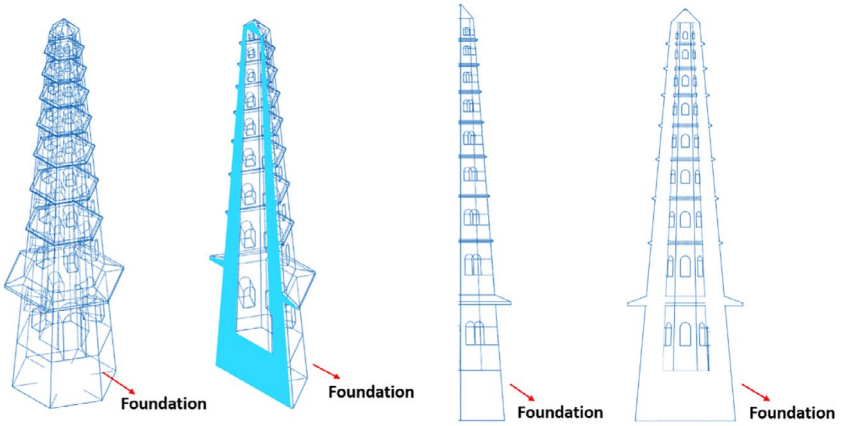

(a1) Physical image (a2) Section view (a3) Elevation a (a4) Elevation view b

(a) Pagoda seismic schematic

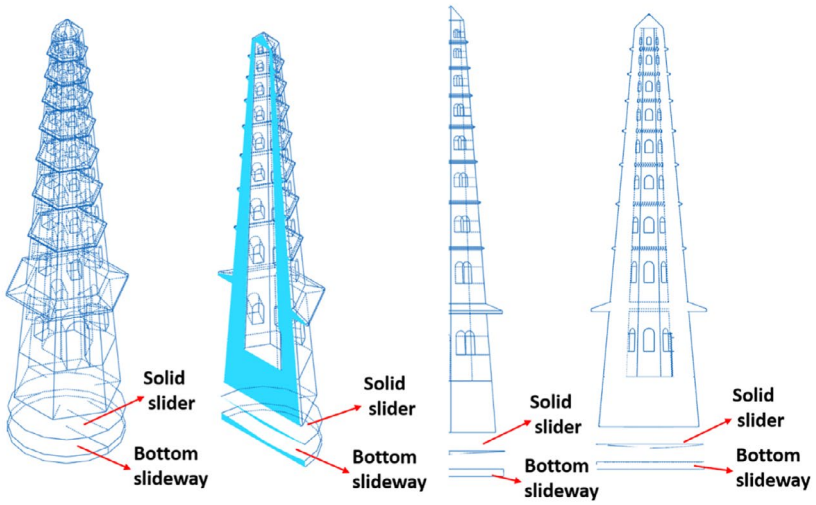

(b1) Physical image (b2) Section view (b3) Elevation a (b4) Elevation view b

(b) Schematic diagram of pagoda OFPB seismic isolation

Fig. 2 Schematic diagram of the pagoda

behavior is defined as hard contact, the tangential behavior is set as penalty friction, and the friction coefficient is 0.01.

Damping calculation

When the structure fights against earthquakes, its existence because of damping can absorb part of the energy brought by earthquakes. In this study, the damping characteristics of the pagoda under seismic action are simulated by the Rayleigh damping model [29], and the damping matrix of the unit is calculated by Eq. 1:

$$[C] = \alpha[M] + \beta[K] \tag{1}$$

where [M] is the mass matrix, [K] is the stiffness matrix, α is the mass damping coefficient, and β is the stiffness damping coefficient. α and β can be obtained from the structural self-resonance frequency ω and the damping ratio ξ, which are computed as shown in Eq. 2:

$$\alpha = \frac{2\xi\omega_i\omega_j}{(\omega_i + \omega_j)}, \beta = \frac{2\xi}{(\omega_i + \omega_j)} \tag{2}$$

In the formula: ωi and ωj are the i and j order self-oscillation frequencies, i = 1 and j = 3 in the text, and ξ is the structural damping ratio. According to the existing research, the damping ratio is taken as 0.04. The self-oscillation frequency of the structure is shown in Table 2.

The empirical formula for the basic period of a masonry structure is shown in Eq. 3 [30]:

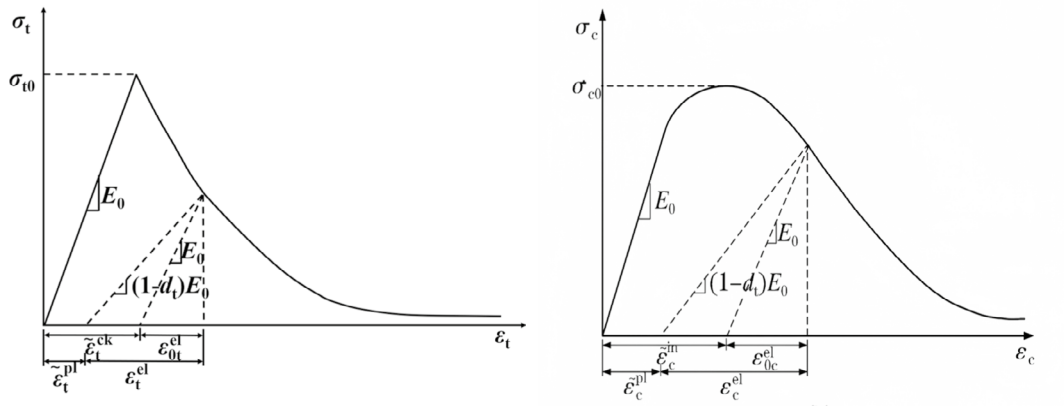

(a) tensile (b) compression

Fig. 3 Schematic of concrete uniaxial tensile and compressive damage and stiffness recover

Table 2 Comparison of the first five natural vibration frequencies of the structure

HZ					
Mode No	**1**	**2**	**3**	**4**	**5**
Pagoda antiseismic	2.467 7	2.467 7	6.807 2	6.807 9	11.522 0
Pagoda isolation	1.651 6	1.651 6	4.445 5	4.446 0	7.680 6

$$T1 = 0.0168(H_0 + 1.2) \tag{3}$$

where H_0 is the height of the structure, and the pagoda height in this study is 22.50 m. The basic period of the seismic structure of the pagoda is calculated as $T1 = 0.0168\ (22.5 + 1.2) = 0.3982$, and the basic period of the seismic structure of the pagoda is calculated as $T1 = 1/2.468 = 0.4052$ according to the simulation results. The difference between the calculated results of Eq. (3) and 1.8% is not large, indicating that the established model can effectively simulate the effect of the pagoda structure.

Selection of earthquakes

The Bai Lang Fengshui Pagoda is located on a site classified as Class II soil, with a seismic intensity of 7 degrees. Considering the special nature of the protection of ancient buildings and the significance of the study, one additional degree was added to the study, and it was determined that the analysis would be carried out by a seismic intensity of 8 degrees. Considering the influence of different epicentral distances, three kinds of earthquakes, near-field earthquake, ordinary earthquake, and far-field earthquake, are selected for study, three earthquakes of each type were selected for analysis based on the structural period, To ensure that the response spectrum of the selected seismic wave is close to the period of the pagoda to ensure the significance of the research content. The selected seismic information is shown in Table 3. The acceleration response spectrum is shown in Fig. 4, and GM-SRS is the canonical response spectrum.

Seismic response analysis

To explore the seismic isolation performance of the overall friction pendulum isolation bearing on the pagoda, three different types of earthquakes were imposed on the seismic model and isolation model respectively, and the X, Y and Z directions of the selected earthquakes were peaked according to 1:0.85:0.65, with the peak value of 4 m/s^2. where the X direction was defined as the east–west direction, the Z direction as the north–south direction, and the Y direction as the vertical direction. The effect of structural damping is described through the damping rate, and the expression is shown in Eq. 4:

$$R = \frac{S_1 - S_2}{S_1} \times 100\% \tag{4}$$

where S1 and S2 represent the seismic response values of seismic resistant and isolated structures respectively.

Results

Acceleration response analysis

Acceleration amplification factor

Figure 5 demonstrates the acceleration magnification factor of the structure. From the figure, it can be seen that the acceleration magnification factors of the two models show consistency, both of which become larger as the height of the pagoda increases, indicating that the acceleration increases as the height of the pagoda rises. Comparing the three types of earthquakes, the acceleration

Table 3 Earthquake information

Earthquake types	No	Earthquake name	Station name	Year	M	Rrup (km)	PGA(X/Y/Z (m*s-2))
Near-Field earthquake	NE-1	Iwate_Japan	IWTH25	2008	6.90	4.80	0.1052/0.4096/0.0275
	NE-2	Imperial Valley-06	Holtville Post Office	1979	6.53	7.50	0.254/0.2215/0.2570
	NE-3	Morgan Hill	Halls Valley	1984	6.19	3.48	0.1551/0.3121/0.1101
Far-Field earthquake	FE-1	Northridge-01	San Bernardino—CSUSB Gr	1994	6.69	103.16	0.2557/0.2217/0.1155
	FE-2	Hector Mine	San Bernardino—Fire Sta. #4	1999	7.13	101.71	0.2314/0.3583/0.1388
	FE-3	Chi-Chi_Taiwan-02	TAP046	1999	5.90	139.62	0.0339/0.0687/0.0207
Common earthquake	CE-1	Northridge-01	LA—Century City CC North	1994	6.69	23.41	0.1162/0.1497/0.0831
	CE-2	Northridge-01	LA—Hollywood Stor FF	1994	6.69	24.03	0.0332/0.04852/0.0487
	CE-3	Northridge-01	San Marino—SW Academy	1994	6.69	35.02	0.0090/0.0076/0.0025

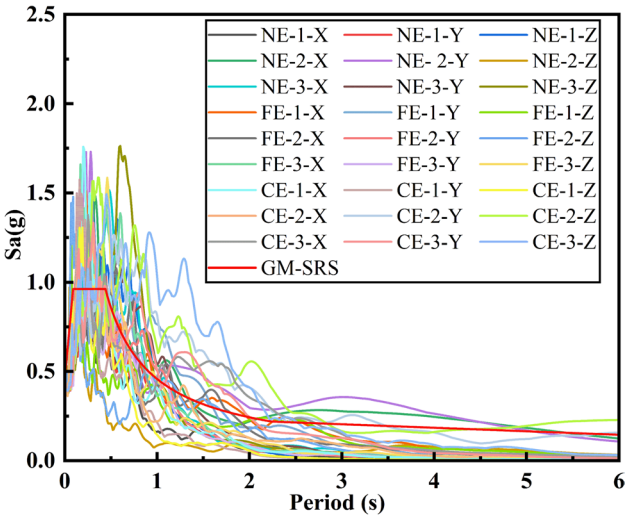

Fig. 4 Seismic acceleration response spectrum

amplification factor of the structure under near-field and far-field earthquakes is larger than that under common seismic operations, indicating that far-field earthquakes and near-field earthquakes are more hazardous to the pagoda. However, the acceleration amplification factor of the pagoda is not much different and is significantly controlled after the seismic isolation using OFPB. Compared with the seismic model, the acceleration amplification factor of the pagoda is reduced by 35.43% to 82.31% for near-field earthquakes, 34.43% to 81.97% for far-field earthquakes, and 34.43% to 81.97% for common seismic operations. The acceleration amplification factor decreases from 30.46 percent to 82.46 percent under common seismic operation. It can be seen that the acceleration of the three seismic waves of the three types has been significantly controlled.

Acceleration time-course analysis

Based on the analyses in the previous section, it can be seen that among the selected seismic waves, the near-field seismic type NE-3 wave, the far-field seismic type FE-1 wave, and the Common seismic type CE-3 wave, have larger values of acceleration response to the structure. Therefore, these three seismic waves are selected to analyze the corresponding top acceleration time course curves of the pagoda. From Fig. 6, it can be seen that

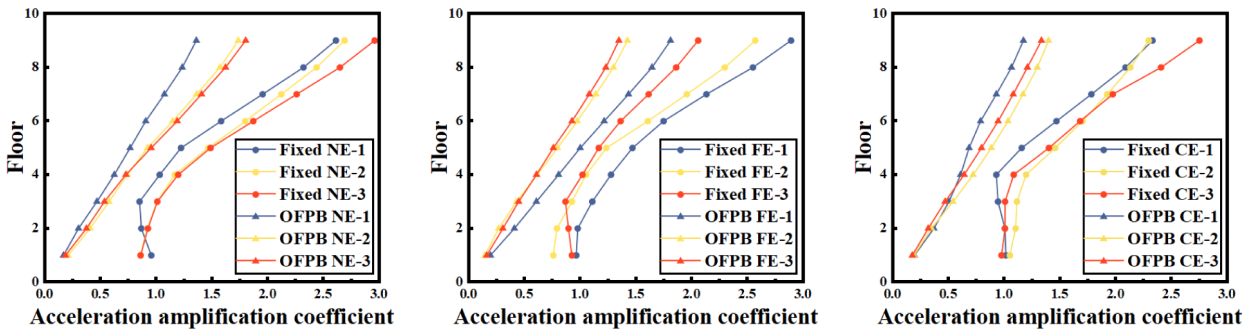

(a)Near-Field earthquake (b)Far-Field earthquake (c)Common earthquake

Fig. 5 Acceleration amplification coefficient

the acceleration response values of the OFPB pagoda isolation structure are effectively reduced under all three types of seismic actions. Under the near-field seismic action, the peak acceleration of the Pagoda seismic structure is 11.84 m/s^2, and the peak acceleration of the OFPB seismic isolation is 7.21 m/s^2, which is reduced by 39.19% in comparison. Under far-field seismicity, the peak acceleration of the Pagoda seismic structure is 11.57 m/s^2, and the peak acceleration of the Pagoda seismic isolation structure is 7.2 m/s^2, which is reduced by 37.77% in comparison. Under Common seismic, the peak acceleration of the pagoda seismic structure is 11.00 m/s^2, and the peak acceleration of the pagoda seismic isolation structure is 5.34 m/s^2, which is reduced by 51.45% in comparison. It can be seen that the top acceleration of the structure is larger under near-field and far-field earthquakes, and the seismic isolation effect of the OFPB is weaker compared to common earthquakes.

Drift response analysis

Floor drift ratio analysis

Figure 7 shows the pagoda's interstorey displacement angle, and the four levels can be used to determine the pagoda's damage level, in which the interstorey displacement angle is less than 1/500, the structure is slightly damaged, the interstorey displacement angle between 1/500 and 1/300, the structure is moderately damaged, the interstorey displacement angle between 1/300 and 1/150, the structure is heavily damaged, and the interstorey displacement is less than 1/150, the structure is on the verge of collapsing.

Comparing the three types of earthquakes, it was found that under both near-field and far-field seismic operations, when the bottom of the pagoda was fixed, the angle of interstorey displacement exceeded 1/150, reaching the level of collapse, and under common seismic operations, the angle of interstorey displacement of the structure tended to be closer to but did not exceed 1/150, which did not reach the level of collapse, but had been seriously damaged. Under OFPB seismic isolation, the pagoda's interstory displacement angle is close to 1/500 or less than 1/500, indicating that the pagoda shows slight damage at most. Under near-field seismic operation, both NE-1 and NE-2 are less than 1/500, indicating no damage to the pagoda, and NE-3 slightly exceeds 1/500, with minor damage to the structure. Under far-field seismic operation, all three waves slightly exceeded 1/500, and all three seismic waves caused minor damage to the pagoda,

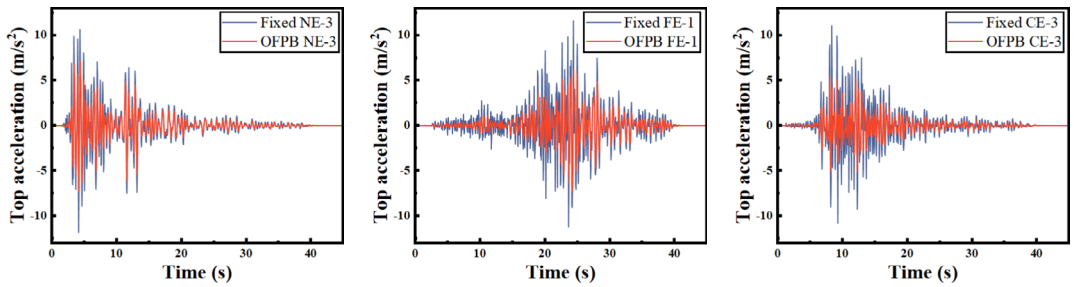

(a)Near-Field earthquake (b)Far-Field earthquake (c)Common earthquake

Fig. 6 Acceleration time history curve

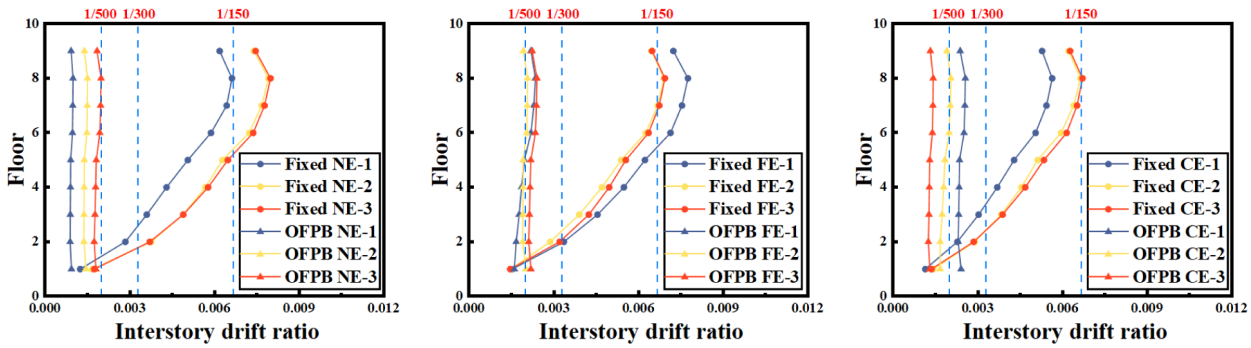

(a)Near-Field earthquake (b)Far-Field earthquake (c)Common earthquake

Fig. 7 Interstory drift ratio

with FE-1 having a greater impact. Under common seismic operation, the interstory displacement angles did not exceed 1/500 for CE-1 and CE-2, and slightly exceeded 1/500 for CE-3, producing minor damage to the structure. It is worth noting that the interstorey displacement angles of the pagoda floors did not change much under the action of OFPB, which indicates that the shear distribution of the floors was uniform. In contrast, the displacement Angle between the lower strata under near-field earthquake action decreases by 85.15%, the displacement Angle between the lower strata under far-field earthquake action decreases by 78.94%, and the displacement Angle between the lower strata under common earthquake action decreases by 70.24%. It can be seen that the reduction rate under ordinary earthquake action is the smallest, which indicates that the more intense the seismic response, the stronger the isolation effect of OFPB. In general, under the action of three types of earthquakes, OFPB plays a significant role in the isolation effect of the pagoda.

Drift time course analysis

Through the analysis in the previous subsection, it can be learned that among the selected seismic waves, the near-field seismic type NE-3 wave, the far-field seismic type FE-1 wave, and the common seismic type CE-3 wave, have larger values of displacement response to the structure. Therefore, these three seismic waves are selected to analyze the corresponding top floor displacement time course curves of the pagoda. By comparing the displacement time histories of the pagoda Fig. 8 shows the displacement time histories of the pagoda under three types of earthquakes, seismic and pagoda isolation models, it is found that under the effect of OFPB isolation, the displacements of the pagoda isolation are in general larger than those of the pagoda seismic isolation, this is due to the fact that the use of OFPB isolation at the bottom, which reduces the constraints of the ground on the pagoda, resulting in larger displacements, but it is this larger displacement, which greatly weakened the displacement due to the But it is this larger displacement that greatly reduces the amount of energy due to the earthquake and ensures less damage to the structure. Due to the friction between the OFPB slider and the slipway, this results in a larger residual displacement of the pagoda compared to the seismic resistance of the pagoda, but this larger residual displacement can be reset by applying an external force to reach the common level.

Shear response analysis

Floor shear analysis

Figure 9 shows the layer shear forces under different types of earthquakes, structurally, the model of the pagoda fixed at the bottom produces a large base shear force, this is due to the fact that the foundation of the pagoda is as high as 2.8 m, which concentrates the gravity at the bottom and there is no seismic isolation measures installed at the bottom, which results in a large base shear force in the structure. The shear force of the pagoda model installed with OFPB bearing is well controlled, especially for the base shear force. In contrast, the installation of OFPB reduces the base shear of the structure by 92.3% to 96.76%, and the shear reduction rate of other layers is also between 20.53% and 49.54%, indicating that OFPB has a significant effect on the seismic isolation of the pagoda.

In terms of different seismic types, the base shear of the pagoda seismic structures under near-field seismic action ranges between 3210.00 kN and 5779.00 kN, and the top shear ranges between 24.85 kN and 30.11 kN. The base shear of the pagoda isolated structure varies between 248.00 kN and 313.00 kN, the top shear varies between 16.4 kN and 23.74 kN, the base shear isolation rate varies between 90.25% and 95.45%, and the shear reduction rate of the other floors varies between 20.53% and 44.16%. The base shear of the pagoda seismic structure under far-field seismic action varies between 2773.00 kN and 6682.00 kN, and the top story shear varies between

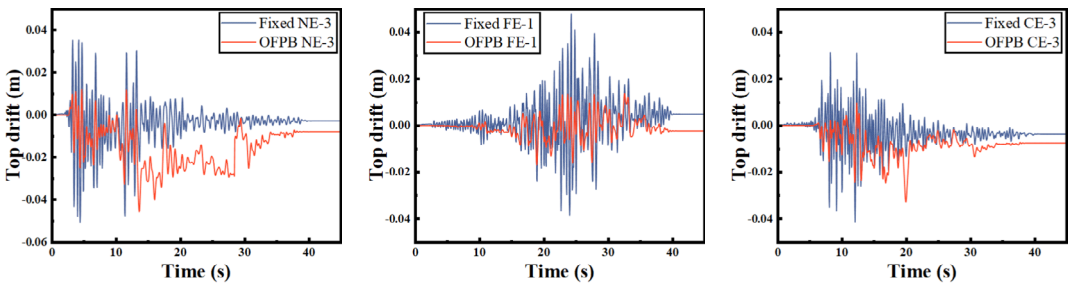

(a)Near-Field earthquake (b)Far-Field earthquake (c)Common earthquake

Fig. 8 Drift time course curve

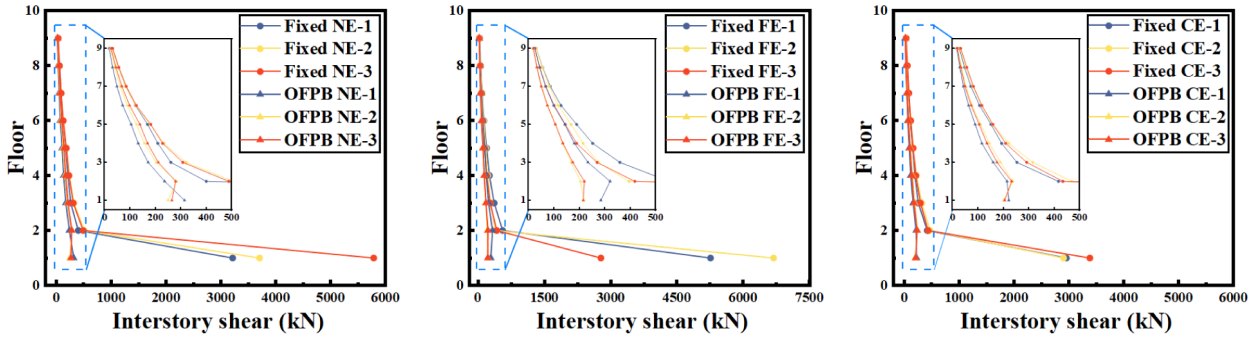

(a)Near-Field earthquake (b)Far-Field earthquake (c)Common earthquake

Fig. 9 Interstory shear

23.04 kN and 28.94 kN. The base shear of the pagoda isolation structure is between 213.60 kN and 282.70 kN, the top shear is between 16.87 kN and 22.74 kN, the base shear isolation rate is between 92.30% and 96.76%, and the shear reduction rate of other layers is between 21.39% and 48.43%. Under the action of ordinary earthquake, the base shear force of the pagoda seismic structure is between 2897.00 kN and 3376.00 kN, and the top shear force is between 30.50 kN and 35.63 kN. The base shear of the pagoda isolation structure is between 198.90 kN and 282.7 kN, the top shear is between 14.80 kN and 22.74 kN, the base shear isolation rate is between 92.55% and 93.98%, and the shear reduction rate of other layers is between 30.19% and 49.54%. In contrast, the response of pagoda under far-field earthquake operation is greater than that under near-field earthquake operation and greater than that under ordinary earthquake action.

Shear time course analysis

According to the analysis in the previous section, it is found that the three earthquakes, NE-3, FE-1 and CE-3, have larger values of shear response to the pagoda, so the time-range curves of these three seismic waves are selected for analysis. Fig. 10 shows the shear time-history curve of the second layer of the pagoda.

When analyzing the dynamic response of the pagoda structure, we noticed that the shear time-history diagram of the second floor showed a response trend consistent with the height of the other floors. Although there are significant differences in the distribution of shear forces in the bottom layer, which makes it difficult to directly reflect this difference in the time history curve, the change in shear forces in the second layer provides us with a valuable perspective. Through careful analysis of the shear time history of this floor, we can reasonably predict the shear changes of other floors under similar dynamic action. This analysis method not only improves our understanding of the overall response of the structure, but also provides us with an effective tool to predict and evaluate the various dynamic load situations that the structure may encounter in practical applications. Through the in-depth study of the second layer shear time history, we can grasp the dynamic characteristics of the structure more accurately, so as to provide solid data support for structural design and safety evaluation.

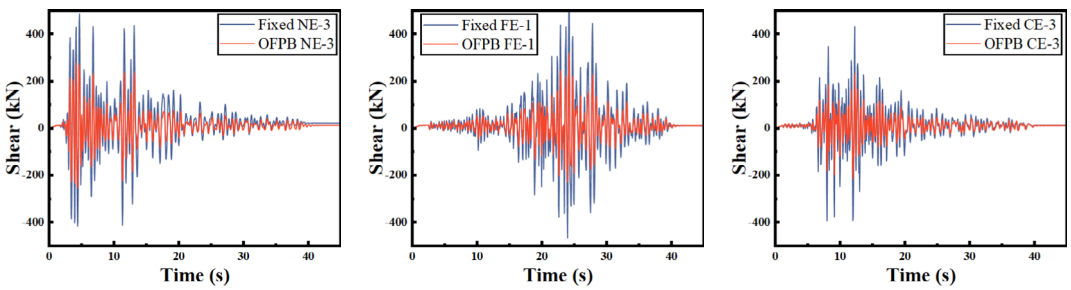

(a)Near-Field earthquake (b)Far-Field earthquake (c)Common earthquake

Fig. 10 Shear time history

Damage response analysis

Damage factor analysis

Because the compressive property of the material is much greater than the tensile property, only the tensile damage behavior of the pagoda is analyzed, and its tensile property is not analyzed this time. The nodes with the greatest damage of the two models are selected, and the tensile damage factors of the two models are compared and analyzed. Fig. 11 shows the variation of damage factors at the node with the maximum damage to the pagoda over time. Under the action of near-field earthquakes, the damage of the structure first reaches the limit value, which appears at the base of the structure, which corresponds to the base shear value of the seismic model of the pagoda. Under the action of the far-field earthquake, the maximum damage node of the pagoda model also reaches the limit value quickly. Finally, under the action of ordinary earthquakes, the maximum damage node of the pagoda model reaches the limit value, which is related to the spectrum distribution of seismic waves. In contrast, the damage factor of the OFPB-isolated structure did not reach the maximum value from the beginning of the earthquake to the end of the earthquake, indicating that the material did not reach the tensile limit value and the structure did not reach the damage condition, which corresponds to the interstorey displacement angle of the isolation model, and the structure only suffered minor damage.

Damage contour of pagoda

According to the analysis of the tensile damage factors of the pagoda in the previous section, NE-3 wave, FE-3 wave and CE-3 wave, which are the most influential near field earthquakes, are selected and the damage under the three types of earthquakes is compared and analyzed. Figure 12 shows the tensile damage diagram of the pagoda seismic model and pagoda isolation model under the action of three types of earthquakes.

Figure 12a, b respectively shows the damage evolution of the pagoda seismic and isolation models under near-field earthquakes. It can be seen that at 2.25 s, large damage occurs at the bottom of the structure [31], and minor damage occurs mainly at the entrance of the upper part, in which the damage near the doorway is greater than that near the bond hole, due to the large shear force at the bottom of the structure, which speeds up the structural failure. At 10.05 s, the damage at the gate of the pagoda was intensified, and the upper part of the gate was almost destroyed, which was due to the weak strength at the entrance of the pagoda, leading to the tensile damage of the structure. At the 40 s, the gate of the pagoda was basically destroyed, and the structure would collapse. On the other hand, the model of the pagoda using OFPB seismic isolation shows only minor damage at the door and coupon openings, which corresponds to the shear diagram of the structure shown in Fig. 9. Since OFPB reduces most of the shear forces at the base of the structure, it allows the foundation part of the structure to be effectively protected, and at the same time, it protects the pagoda from being damaged.

Figure 12c, d shows the tensile damage diagrams of the seismic and isolation models of the Pagoda under far-field seismic effects. It can be seen that at 8.5 s the base of the pagoda's foundation appears slight damage, at 20.50 s, the tensile damage begins to appear on the side of the pagoda's doorway, the second and third floor coupon holes appear smaller damage, this is due to the fact that these parts are in the weaker part of the strength of the place, which leads to the structure to be subjected to larger tensile force, when the earthquake comes to 40 s, the damage of the pagoda's first floor, the third floor, and the fourth floor holes continue to increase to the limiting value, and the structure has a probability of collapse. Comparing the damage of the pagoda under OFPB isolation, only slight damage occurs at the opening of the first floor at 40 s, which shows that the pagoda is effectively protected under the far-field seismic action.

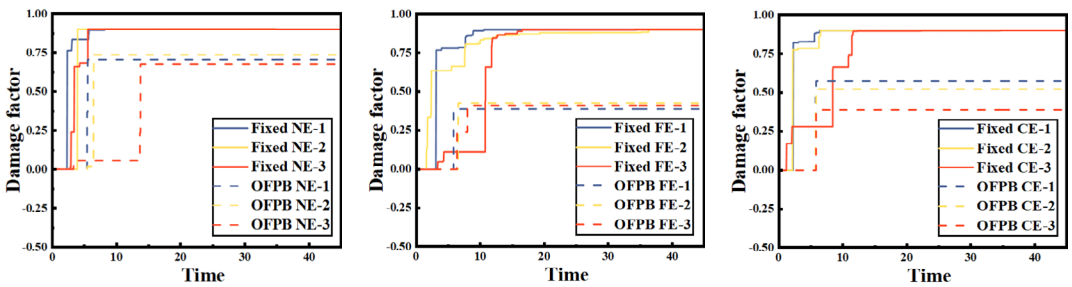

(a)Near-Field earthquake (b)Far-Field earthquake (c)Common earthquake

Fig. 11 Tensile damage factor time history

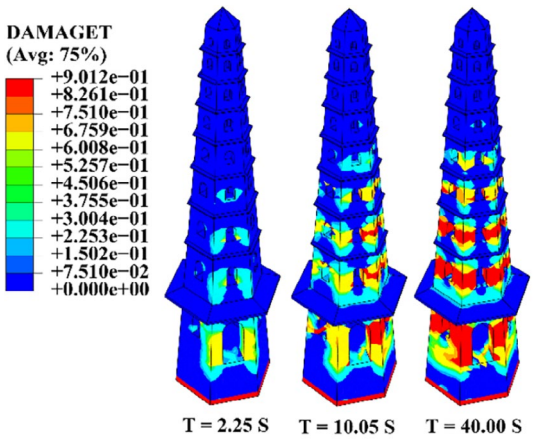

(a)Fixed NE-3

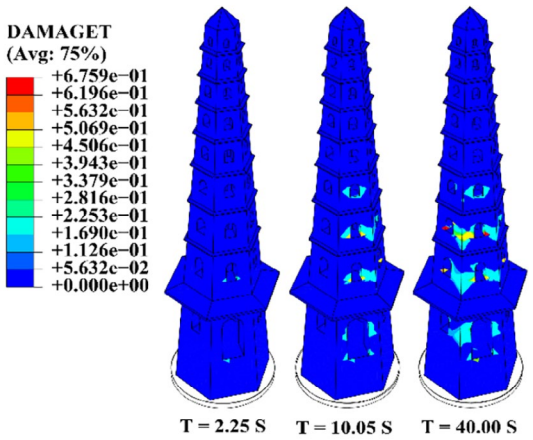

(b)OFPB NE-3

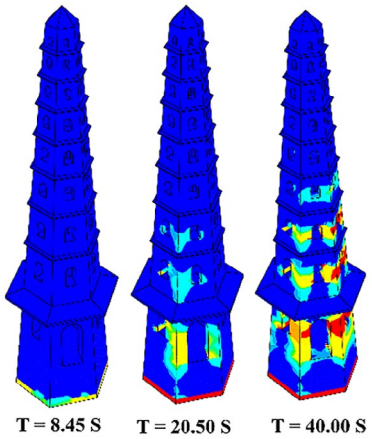

(c)Fixed FE-3

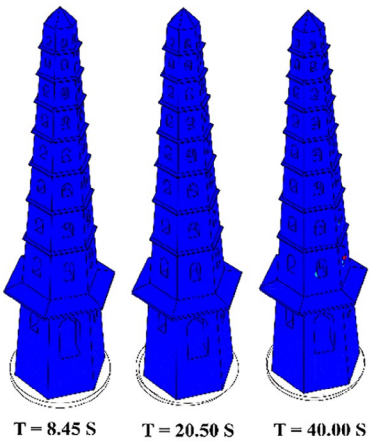

(d)OFPB FE-3

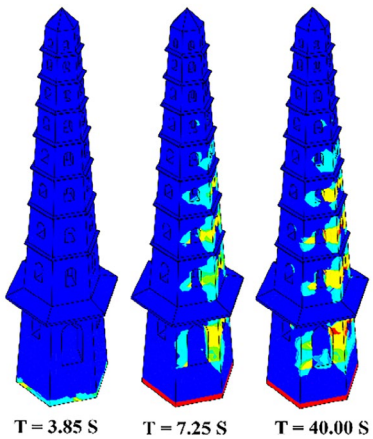

(e)Fixed CE-3

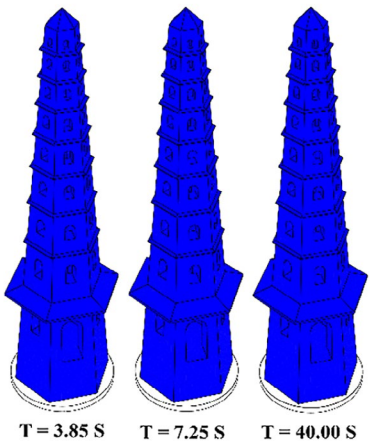

(f)OFPB CE-3

Fig. 12 Comparison of Pagoda Tension Damage

Figure 12e, f shows the tensile damage of the Pagoda seismic and seismic isolation models under common seismic action, at 3.85 s, the slight damage at the bottom of the Pagoda foundation starts to appear, and the overall damage has not yet appeared, at 7.25 s, the damage at the bottom of the foundation expands, and spreads to the edges of the opening of the coupon hole at the same time, and at 40 s, the damage of the Pagoda continues to increase, and partially reaches the damage limit value. On the contrary, in the seismic isolation model of the pagoda, the structure did not show any obvious damage. In contrast, the damage of the pagoda under the near-field earthquake is the largest, and the pagoda is on the verge of collapse, the damage under the far-field earthquake is larger, and the pagoda has the probability of collapse, and the damage of the pagoda is smaller under the common earthquake, which may be due to the fact that the frequency of near-field earthquakes is more likely to be close to the pagoda's natural frequency, which leads to the pagoda's resonance effect, and thus exacerbates the damage of the pagoda.

Conclusion

To protect ancient pagodas in earthquake-prone areas, this study adopts OFPB to isolate pagodas, which effectively guarantees the integrity of pagodas and aims to highlight the protection of pagodas without damaging them, and three types of seismic response analysis were carried out on the two models respectively, including near-field earthquake, far-field earthquake and ordinary earthquake. Each type of earthquake was analyzed through three seismic waves. The acceleration response, displacement response, shear response and damage response of the two structures are analyzed and compared. The following conclusions are drawn:

(1) Importance of seismic isolation technology in pagoda protection: The application of overall friction pendulum bearing (OFPB) seismic isolation technology in pagoda structures significantly reduces the structural response to seismic action. By effectively isolating the seismic energy, this technique significantly reduces the acceleration amplification factor, inter-story displacement, base shear force, and tensile damage of the pagoda in earthquakes, thus significantly improving the seismic performance and safety of the structure. The application of seismic isolation technology not only protects the structural integrity of the pagoda, but also preserves its historical and cultural value, which is of great practical significance for the protection of pagodas in earthquake-prone areas.

(2) Effect of type of earthquake on structural response: It was noted that the response of the pagoda under near-field and far-field earthquakes was greater than that of normal earthquakes. This finding emphasizes the importance of the type of earthquake on the seismic design of the structure. Near-field earthquakes may result in greater structural response due to their strong ground motion and short period characteristics. Therefore, special consideration needs to be given to the effects of near-field earthquakes in seismic design to ensure that the structure remains stable and safe under all seismic conditions.

(3) Universality and efficiency of seismic isolation technology: Pagodas with overall friction pendulum bearing isolation show significant isolation effects under near-field, far-field, and normal seismic effects. This indicates that the isolation technique is not only applicable to specific types of earthquakes, but also has wide universality. By reducing the transfer of seismic energy to the superstructure, the seismic isolation technique effectively reduces the risk of earthquake damage to the pagoda and improves its seismic capacity. The high efficiency of this technology provides an effective solution for the protection of important cultural heritage sites such as the Pagoda and helps to reduce the damage caused by seismic hazards.

Acknowledgements
The writers gratefully acknowledge the financial support of National Natural Science Fund of China (No.52168072 & No.51808467), High-level Talent Support Project of Yunnan Province, China(2020).

Author contributions
QH collected pagoda parameters, wrote the main manuscript text and drew Figs. 2, 3, 4, 5, 6, 7, 8, 9, 10, 11, 12; DwL provides research ideas and financial assistance for overall friction pendulum isolation bearing (OFPB); ML provides resources and ideas; XpL builds the pagoda model shown in Fig. 2; HxW gives the contents of Fig. 1. All authors reviewed the manuscript.

Funding
This research was funded by National Natural Science Fund of China (Nos. 52168072, 51808467), High-level Talent Support Project of Yunnan Province, China(2020).

Availability of data and materials
No datasets were generated or analysed during the current study.

Declarations

Competing interests
The authors declare no competing interests.

Received: 21 July 2024 Accepted: 8 September 2024
Published online: 13 September 2024

References

1. Zhang S, Liang J, Su X, Chen Y, Wei Q. Research on global cultural heritage tourism based on bibliometric analysis. Herit Sci. 2023;11:139. https://doi.org/10.1186/s40494-023-00981-w.
2. Bartoli G, Betti M, Giordano S. *In situ* static and dynamic investigations on the "*Torre Grossa*" masonry tower. Eng Struct. 2013;52:718–33. https://doi.org/10.1016/j.engstruct.2013.01.030.
3. Bennati S, Nardini L, Salvatore W. Dynamic behavior of a medieval masonry bell tower. part I: experimental measurements and modeling of bell's dynamic actions. J Struct Eng. 2005;131:1647–55. https://doi.org/10.1061/(ASCE)0733-9445(2005)131:11(1647).
4. Puncello I, Caprili S. Seismic assessment of historical masonry buildings at different scale levels: a review. Appl Sci. 2023;13:1941. https://doi.org/10.3390/app13031941.
5. Chávez M, Meli R. Shaking table testing and numerical simulation of the seismic response of a typical Mexican colonial temple. Earthquake Eng Struct Dynam. 2012;41:233–53. https://doi.org/10.1002/eqe.1127.
6. Anzani A, Binda L, Carpinteri A, Invernizzi S, Lacidogna G. A multilevel approach for the damage assessment of historic masonry towers. J Cult Herit. 2010;11:459–70. https://doi.org/10.1016/j.culher.2009.11.008.
7. Lee G, Park H-J, Pham KVA, Kim J-Y, Lee S-M, Lee K. Evaluation of seismic performance of masonry stone pagoda: dynamic centrifuge test and numerical simulation analysis. Sustainability. 2023;15:13098. https://doi.org/10.3390/su151713098.
8. De Iasio A, Wang P, Scacco J, Milani G, Li S. Longhu pagoda: advanced numerical investigations for assessing performance at failure under horizontal loads. Eng Struct. 2021;244: 112715. https://doi.org/10.1016/j.engstruct.2021.112715.
9. Shakya M, Varum H, Vicente R, Costa A. Seismic vulnerability and loss assessment of the Nepalese Pagoda temples. Bull Earthq Eng. 2015;13:2197–223. https://doi.org/10.1007/s10518-014-9699-5.
10. Lu J, Han X, Wang Z, Li C. Research on dynamic properties of ancient masonry pagoda with solid structure in China. Int J Archit Herit. 2022;16:746–66. https://doi.org/10.1080/15583058.2020.1845417.
11. Wang P, Milani G, Scuro C, Demarco F, Olivito RS, Li S. Simulation and Fast vulnerability analysis of a Chinese masonry pagoda. J Phys: Conf Ser. 2022;2204: 012046. https://doi.org/10.1088/1742-6596/2204/1/012046.
12. Ponsi F, Bassoli E, Vincenzi L. Bayesian and deterministic surrogate-assisted approaches for model updating of historical masonry towers. J Civ Struct Heal Monit. 2022;12:1469–92. https://doi.org/10.1007/s13349-022-00594-0.
13. Lu J, Zhang C, Wang Z, Han X. Dynamic performance and seismic damage analysis of an ancient masonry pagoda. J Asian Archit Buil Eng. 2022;21:2009–26. https://doi.org/10.1080/13467581.2021.1971677.
14. Lu J, Han X, Wang Z, Li C. Research on dynamic properties of ancient masonry pagoda with solid structure in China. Int J Archit Herit. 2022;16:746–66. https://doi.org/10.1080/15583058.2020.1845417.
15. Wu X, Lu J, Wang Z, Yang W, Qiao N. Dynamic characteristics and seismic response analysis of the bottle-shaped masonry ancient pagoda. Structures. 2022;44:1648–59. https://doi.org/10.1016/j.istruc.2022.08.109.
16. Wang P, Milani G. Specialized 3D Distinct element limit analysis approach for a fast seismic vulnerability evaluation of massive masonry structures: application on traditional pagodas. Eng Struct. 2023;282: 115792. https://doi.org/10.1016/j.engstruct.2023.115792.
17. Xu D, Xie Q, Zhang Y, Hao W. Effects of inclination on the seismic performance of Chinese historical masonry tower identified through shaking table tests. J Earthquake Eng. 2023;27:1458–81. https://doi.org/10.1080/13632469.2022.2074573.
18. Li M, Lu J, Wu X, Wang D. Discrete element analysis of dynamic characteristics and earthquake collapse of solid structure ancient masonry pagoda. Structures. 2023;57: 105208. https://doi.org/10.1016/j.istruc.2023.105208.
19. Tian P, Yang W, Lu J, Wu X, Wang Z. Study on the shear properties of masonry pagoda mortar and its influencing factors. Case Stud Const Mater. 2024;20: e02981. https://doi.org/10.1016/j.cscm.2024.e02981.
20. Hu J, Zhou J, Wang S, Sun M, Chen H, Li X. In situ testing and FEM analysis of dynamic characteristics of a masonry pagoda under natural excitation. Buildings. 2024;14:1700. https://doi.org/10.3390/buildings14061700.
21. Xie Q, Xu D, Zhang Y, Yu Y, Hao W. Shaking table testing and numerical simulation of the seismic response of a typical China ancient masonry tower. Bull Earthq Eng. 2020;18:331–55. https://doi.org/10.1007/s10518-019-00731-z.
22. Pham KVA, Hong S-G, Lee S-M, Park H-J, Lee K. Assessment of seismic performance of three-story masonry stone pagoda by dynamic centrifuge test and simulation analysis. Int J Archit Herit. 2021;15:1213–26. https://doi.org/10.1080/15583058.2019.1665143.
23. Tang YJ, Zhao Y. Leaning pagodas in China: laboratory test and analysis of subsidence under frequent earthquakes. Bull Eng Geol Environ. 2018;77:823–35. https://doi.org/10.1007/s10064-016-0993-0.
24. Li SW, Wei JW, Li TY, Li QM, Bell AJ. Assessment of repairs and strengthening of a historic masonry pagoda using a vibration-based-method. J Struct Eng. 2009;135:67–77. https://doi.org/10.1061/(ASCE)0733-9445(2009)135:1(67).
25. Mason JA. Strengthening of a historic unreinforced masonry church tower. Pract Period Struct Des Constr. 2008;13:31–8. https://doi.org/10.1061/(ASCE)1084-0680(2008)13:1(31).
26. Li T, Wang S, Yang T. Experiment and simulation study on vibration control of an ancient pagoda with damping devices. Int J Struct Stab Dyn. 2018. https://doi.org/10.1142/S0219455418501201.
27. Hao W, Xie Q, Xu D, Zhang Y. Seismic performance of the ancient pagoda wall strengthened with GFRP bars embedded in the horizontal mortar joint under in-plane cyclic loading. J Buil Eng. 2022;51: 104299. https://doi.org/10.1016/j.jobe.2022.104299.
28. Yi PAN, Zichao W, Feng S, Qingzi GE, Shuang Y. Study on isolated reinforcement scheme of ancient masonry pagoda in Sichuan province. J Southwest Jiaotong Univer. 2018;53:540–7. https://doi.org/10.3969/j.issn.0258-2724.2018.03.015.
29. Kwok AOL, Stewart JP, Hashash YMA, Matasovic N, Pyke R, Wang Z, et al. Use of exact solutions of wave propagation problems to guide implementation of nonlinear seismic ground response analysis procedures. J Geotechn Geoenviron Eng. 2007;133:1385–98. https://doi.org/10.1061/(ASCE)1090-0241(2007)133:11(1385).
30. Ma P. Analyzing seismic behavior and micro-modeling of masonry walls using ABAQUS software. Multisc Multidis Model Exp Des. 2024. https://doi.org/10.1007/s41939-023-00344-9.
31. Lu J, Zhang C, Wang Z, Han X. Dynamic performance and seismic damage analysis of an ancient masonry pagoda. J Asian Archit Buil Eng. 2021. https://doi.org/10.1080/13467581.2021.1971677.

Publisher's Note